Influence of Element Substitution on the Cluster Arrangement in the Novel Structures Ca3Tl5, Sr3Tl5, and Sr3Sn5–xTlx (x = 1.8 and 2.2)

Thomas F. Faessler

Zeitschrift für Anorganische und Allgemeine Chemie

Influence of Element Substitution on the Cluster Arrangement in the Novel Structures Ca3Tl5, Sr3Tl5, and Sr3Sn5−xTlx (x = 1.8 and 2.2)

Journal:	*Zeitschrift für Anorganische und Allgemeine Chemie*
Manuscript ID:	zaac.200900210.R2
Wiley - Manuscript type:	Article
Date Submitted by the Author:	27-May-2009
Complete List of Authors:	Faessler, Thomas; Technische Universitaet Muenchen, Department Chemie
Keywords:	Cluster compounds, Tin, Electronic structure, Intermetallic phases, Thallium

Influence of Element Substitution on the Cluster Arrangement in the Novel Structures Ca_3Tl_5, Sr_3Tl_5, and $Sr_3Sn_{5-x}Tl_x$ (x = 1.8 and 2.2)

Sung-Jin Kim and Thomas F. Fässler*

Department Chemie, Technische Universität München.

Dedicated to Professor Martin Jansen on the occasion of his 65th birthday

Abstract

The compounds $Sr_3Sn_{5-x}Tl_x$ (x = 1.78(4), **I**; 2.16(5), **II**), Ca_3Tl_5 (**III**), and Sr_3Tl_5 (**IV**) have been obtained by direct fusion of the elements in sealed Nb ampoules at high temperature. Their structures were determined by single crystal X–ray diffraction studies and the bonding was investigated by *TB–LMTO–ASA* calculations. The ternary phases **I** and **II** crystallize in the Tm_3Ga_5 structure type; space group *Pnma* (No. 62); Z = 4 with a = 13.422(1), b = 10.897(1), c = 6.897(1) Å for **I** and a = 13.482(2), b = 10.938(2), c = 6.850(1) Å for **II**. The binary compounds **III** and **IV** crystallize in the Pu_3Pd_5 structure type; space group *Cmcm* (No. 63); Z = 4 with a = 10.231(2), b = 8.362(2), c = 10.623(2) Å for **III** and a = 10.592(5), b = 8.667(5), c = 10.973(6) Å for **IV**. Both structure types consist of zigzag chains of distorted square pyramidal $\{E_5\}$ (E = Tl, Sn/Tl) clusters. In the lower symmetric structures **I/II** the clusters are reoriented with respect to each other and have only two *exo*–contacts each, whereas in **III/IV** the clusters are aligned parallel and show a considerably higher degree of polymerization. The DOS for $Sr_3Sn_{5-x}Tl_x$ calculated for x = 0 reveals a pseudo gap for x = 2 within the rigid band model, whereas the electronic band structure for Sr_3Tl_5 and Ca_3Tl_5 show metallic properties and strong participation of the cations in the bonding.

Keywords: Cluster compounds, Crystal structure, Electronic structure, Intermetallic phases, Thallium, Tin

* Prof. Dr. Thomas F. Fässler
Department Chemie, Technische Universität München,
Lichtenbergstr. 4, D–85747 Garching, Germany.
E–mail: Thomas.Faessler@lrz.tum.de

1. Introduction

Among the classes of inorganic solids, intermetallic compounds are the ones that are least understood with respect to their bonding properties [1]. This is mainly due to the fact that some of the features that primarily determine the chemical bond, such as the degree of valence electron transfer and electron localization, vary strongly and almost continuously with composition and the nature of the elements involved [2–5]. Connected to the problem of chemical bonding is the difficulty to understand why specific structures occur and how these structures are related to the specific physical properties. Many examples show the gradual transition from valence compounds to typical intermetallic phases. This transition is dependent on the electronegativity difference, the valence electron concentration (*vec*), cation–anion interactions, and packing efficiency [5-11]. For investigation of the dominant structure directing factors the strategy of atom for atom substitution is a valuable experimental tool [12,13].

Due to the remarkable property of tin to establish covalent and metallic bonding in intermetallic compounds [11] we are focused on substitution effects in binary *Ae* (*Ae* = alkaline earth metal) stannides, such as $BaSn_3$ [13,14], $SrSn_3$ [15], $SrSn_4$ [16], and $BaSn_5$[17]. In particular the phases Ae_3Sn_5 (*Ae* = Sr, Ba, Pu_3Pd_5–type) [18,19] in which the tin atoms form five–atom clusters with weak interactions between them (shortest intercluster distances are 3.40 and 3.69 Å, respectively) represent interesting case studies: In these compounds the *Zintl* formalism [20] might be extended by the electron–counting scheme according to *Wade's* rules [21]. Electron transfer from the *Ae* atoms to tin leads to the polyanion $\{Sn_5\}^{6-}$, which has an *arachno*–type structure and derives from a pentagonal bipyramid by removing two adjacent cluster vertices. However, band structure calculations show that these compounds are metallic and two excess electrons occupy antibonding cluster orbitals. Several substitution investigations in this system have been reported: Phase stability in the $Ae_3(Tr/Tt)_5$ systems (*Tr* = In, Al; *Tt* = Pb) by adjusting the *vec*/*E* (*E* = *Tr*/*Tt*) and the effect of relative atom sizes has been studied [22]. Further, tetrel for tetrel substitution in the compound $Ba_3Ge_{2.82}Sn_{2.18}$ preserving the Pu_3Pd_5–type [18] and the role of the cations in the formation of different Zintl polyanions has been investigated [23]. The clusters in the formally two electron deficient Eu_3Ge_5 have even a barrelane-like shape [24].

Similar five atom triel clusters have been found in RE_3In_5 (*RE* = La, Y) [25] and RE_3Ga_5 (*RE* = Sc, Y, Tb–Tm, Lu). The latter Ga compounds crystallize with Tm_3Ga_5–type [26] (Figure 1a) and show reorientation of the five atom clusters (with respect to their alignment in the Pu_3Pd_5 type, Figure 1b). Noteworthy, Sr_3In_5 [27] (*vec*/In = 2.63) crystallizes in the

completely different $Hf_3Ni_2Si_3$ [28] structure type which contains a network of two– (2*b*) and four–bonded (4*b*) In atoms (Table 1).

Recently, we reported about the breakdown of the anionic Sn substructure on the substitution with Bi in the $Ae_3Sn_{5-x}Bi_x$ (*Ae* = Sr, Ba) phases [29]. Focusing on the effect of *vec* in the pyramidal $\{Sn_5\}^{6-}$ clusters we extended our partial substitutions also to electron poorer elements in which we aimed to remove the extra cluster electrons and to attain isolated *nido*–cluster with 14 skeletal electrons. Herein, we report on the synthesis and characterization of the novel phases $Sr_3Sn_{5-x}Tl_x$ (x = 1.78 (**I**), 2.16 (**II**)), Ca_3Tl_5 (**III**), and Sr_3Tl_5 (**IV**). With respect to the binary phase Sr_3Sn_5 the partially substituted phases (**I**, **II**) show a cluster reorientation whereas the fully substituted compounds (**III**, **IV**) return to the higher symmetric structure of the parent phase.

2. Experimental Section

2.1 Synthesis. All manipulations were performed inside an argon–filled glove box (O_2/H_2O levels ≤ 0.1 ppm). The starting chemicals were commercially obtained: Sr 98+% (Chempur); Ca 99.5% (Riedel–de–haän); Sn 99,99% (Merck); In 99.99% (Aldrich); Tl 99.95% (ABCR). Stoichiometric amounts were placed into niobium ampoules which were sealed and enclosed into evacuated silica tubes. Afterwards the following temperature treatments were conducted:

For **I** and **II** the mixtures were heated to 750 °C at a rate of $2K \cdot min^{-1}$. Homogenization at that temperature for 6 h was followed by slow cooling to 500 °C (rate 0.1 $K \cdot min^{-1}$) and annealing there for five days. Compound **I** was first obtained from a loading '$Sr_3Sn_{3.5}Tl_{1.5}$' and **II** from a Tl–rich loading '$Sr_3Sn_{1.5}Tl_7$'. Tl–poorer loadings, such as $Sr_3Sn_{3.5}Tl_y$ ' with y < 1.5 led to the formation of products mainly consisting of phases with compositions such as $SrSn_{1.25}Tl_{1.75(3)}$, which like $BaSn_3$ [12], crystallize in the Ni_3Sn structure type. An indium analogue was prepared form a loading '$Sr_3Sn_3In_2$' using the same temperature treatment. Although In and Sn are not distinguishable by X–rays, from that reaction, we refined a single crystal with nominal crystallographic composition $Sr_3Sn_{3.8}In_{1.2(3)}$: Space group *Pnma*, a = 13.349(3), b = 10.857(3), c = 6.883(2) Å, V = 997.6(5) $Å^3$, and R_1 / wR_2 (all data) = 0.030 / 0.047. Attempts to synthesize Ba analogues by reacting loadings of stoichiometric mixtures, such as 'Ba_3SnTl_4', '$Ba_3Sn_{1.5}Tl_{3.5}$', or '$Ba_3Sn_2Tl_3$' were unsuccessful and resulted in mixtures of Ba_3Sn_5 and $BaSn_{3-x}Tl_x$ (Ni_3Sn–type). **III** and **IV** were obtained from loadings by heating to 940 °C at a rate of $2K \cdot min^{-1}$. The reaction at that temperature took place for 6 h and was followed by cooling to 600 °C at the same rate and annealing there for seven days.

Phase analysis of all products was done by X–ray powder diffraction using a Stoe STADI P2 diffractometer (Ge(111) monochromator for Cu–Kα_1 radiation: λ = 1.54056 Å) equipped with a linear position sensitive detector. For sample preparation, the products of reactions using stoichiometric loadings were finely ground in an agate mortar, diluted with diamond powder, and filled into glass capillaries which then were sealed using a hot tungsten wire. The samples were measured in Debye–Scherrer mode ($2\theta_{max}$ = 80°), and the data analysis was done using the Stoe *WinXPOW* software package. By comparing experimental and calculated powder patterns from the single crystal refinements the phases were successfully identified. The compounds appear as single phase products, however for compounds **IV** and **V**, $CaTl_3$ [30] and $SrTl_2$ [31], respectively, were present as byproducts.

2.2 EDX Analysis. Semi quantitative EDX analysis of different crystallites were carried out by use of a JEOL 5900LV electron microscope system operating at 20 kV and equipped with a Röntec EDX detector. Inside the glove box, several crystallites from each reaction were fixed onto an aluminum sample holder with carbon tape. During transfer of the samples into the microscope chamber they were shortly exposed to air. Thus, images from secondary electrons revealed partial surface oxidation but enough smooth areas were available for the measurements. Analysis of three spots per crystallite with a counting time of three minutes for each spot showed fair agreements in average atomic compositions (at–%, standard deviations of the last integer are given in brackets) of *Ae* : Tl : Sn for **I**: 32(3) : 47(5) : 21(2) (expected values: 37.5 / 40.3 / 22.3); for **II**: 34(2) : 37(2) : 29(4) (expected values: 37.5 : 35.5 : 27); for **III**: 34(3) : 66(6) : 0 (expected values: 37.5 : 62.5 : 0); and for **IV**: 37(4) : 63(5) : 0 (expected values: 37.5 : 62.5 : 0).

2.3 Single Crystal Structure Determinations. For all four compounds the relevant crystallographic and refinement details are listed in Table 2. Table 3 contains the atomic positions and equivalent displacement parameters and Table 4 shows selected interatomic distances. For each compound one block shaped crystal with silvery metallic luster was fixed on a glass tip and sealed in a capillary inside the glove box.

For compounds **I** and **II** the diffraction data were collected at room temperature on a Oxford Xcalibur3 diffractometer using Mo–K$_\alpha$ radiation (λ = 0.71073 Å, graphite monochromator, CCD detector). 416 frames were collected in four omega scans with 20 s exposure time per frame. After applying empirical absorption corrections [32] the structures were solved and refined anisotropically in the space group *Pnma* with *SHELX* [33]. For both compounds four Sn and two Sr positions were found and the model significantly improved by introducing mixed occupied *M* = Sn / Tl sites.

Data collections for compounds **III** and **IV** were carried out at room temperature on a Stoe IPDS 2T diffractometer (λ = 0.71073 Å, graphite monochromator, image plate detector) at the window of a rotating anode (Bruker Nonius FR 591). 180 frames were collected in two omega scans with 10 min exposure times per frame. After applying numerical absorption corrections using the *X-Shape* and *X-Red* program packages [34] the structures were solved and refined in the orthorhombic space group *Cmcm* with *SHELX*. For both datasets three Tl and two *Ae* positions were found and refined anisotropically. Further details of the crystal structures investigations can be obtained from Fachinformationszentrum Karlsruhe, 76344 Eggenstein–Leopoldshafen, Germany, (fax: (+49)7247–808–666; e–mail: crysdata@fiz–karlsruhe.de) on quoting the depository numbers CSD 380327 (**I**), CSD 380326 (**II**), CSD 380324 (**III**), and CSD 380325 (**IV**).

2.4 Electronic Structure. Self–consistent band structure calculations for **II – IV** were performed with the linear–muffin–tin–orbital (LMTO) method using the Stuttgart *LMTO47c* program code [35]. Scalar relativistic corrections were included. The band structure of $Sr_3Sn_{5-x}Tl_x$ (**II**) was calculated for x = 0 using the lattice parameters and space group of compound **II**. *k*–space integration was performed by the tetrahedron method on sets of 365 irreducible *k* points and a basis set with Ca–4*s*/(4*p*)/4*d*, Sr–5*s*/(5*p*)/4*d*/(4*f*), Sn–5*s*/5*p*/(5*d*)/(4*f*), and Tl–6*s*/6*p*/(6*d*)/(5*f*) ("downfolded" [36] orbitals in parentheses). For space filling within the atomic sphere approximation, interstitial spheres were introduced in order to avoid too large overlap of the atom–centered spheres. The empty spheres (ES) positions and radii were calculated automatically within the limit of 18% overlap with any atom–centered spheres. WS radii [a.u.] were: Ca: 3.56–3.83; Sr: 3.68–4.16; Tl: 3.36–3.54; Sn: 3.30–3.42; ES: 1.39–1.68. The crystal orbital *Hamilton* population (COHP) [37] method was used for the analysis of bonding interactions. The Fermi level in all figures is set to zero and the COHP diagrams are drawn by reversing their values with respect to the energy scale (i. e. –COHP *vs*. *E*). By this the calculated peak values become negative for antibonding and positive for bonding interactions.

3. Results and Discussion

The title compounds are distributed to two A_3B_5 structure types, as listed in Table 1. Whereas $Sr_3Sn_{5-x}Tl_x$ for **I** (x = 1.78) and **II** (x = 2.16) adopt the Tm_3Ga_5 type (Figure 1a), phases Ca_3Tl_5 (**III**) and Sr_3Tl_5 (**IV**) crystallize in the Pu_3Pd_5 structure (Figure 1c). Both structure types feature slightly irregular square planar pyramids in their anionic parts. In the Pu_3Pd_5 types the basal planes of these clusters are all oriented parallel approximately to the *ac* plane and the apex atoms of the pyramids point up [0 1 0] and down [0 −1 0]. Inclusion of the shortest intercluster distances between the atoms of the basal plane generates parallel zigzag chains of clusters that are primitively stacked along *b* (**Figure 1c**). Contrary, in the Tm_3Ga_5 type phases the cluster chains alternate with respect to the chain tilt angle along the *a* direction (**Figure 1a**) resulting in a herringbone pattern arrangement. This observation of different stacking variants is reminiscent of the different alignments of zigzag chains of atoms in CrB and FeB [38].

3.1 Structure Description for I and II. The compounds crystallize in the Tm_3Ga_5 [26] structure type with a statistical occupation of Tl and Sn at the Ga positions (Table 3). A projection of the unit cell of $Sr_3Sn_{3.22}Tl_{1.78(4)}$ (**I**), as a representative for both compounds, is shown in Figure 1a. The *M* = Sn / Tl (*M*1 to *M*4) atoms form approximated square pyramidal clusters with M2–M3–M3–M4 forming the basal planes and M1 the apex atoms (Figure 2). The clusters are interconnected *via* longer *M*3–*M*3 intercluster bonds along *b* (Table 4) and compared to those of Pu_3Pd_5–type, such as in Ae_3Sn_5 (*Ae* = Sr, Ba; Figure 1b), their alignment only differs in terms of the relative arrangement of the as formed zigzag chains of clusters relative to the *a* axis. Therefore, the clusters in the ternary phases occur in an arrangement of lower symmetry then in the binary phases: The cluster chains are tilted with respect to the *a* axis by ±36.3° and ±35.7° for **I** and **II**, respectively. Between the clusters one set of intercluster bonds is present at 3.43 (3.45) Å for **I** (**II**) which leads to two *exo*–bonds per cluster (Figure 2a). Among these, the next nearest *exo*–contacts are at distances ranging from 3.83–4.83 (3.73–4.84) Å. The highest site occupancies of Sn are observed at the *M*2 (70% in **I** and 56% in **II**) and at the *M*3 sites (78% in **I**, 76% in **II**). This distribution is consistent with the fact that the more electronegative Sn (X_{Tl} = 1.62, X_{Sn} = 1.96, *Pauling* scale [39]) is preferentially located at sites with lower coordination numbers. This observation of 'topological charge stabilization' has been discussed for many other 'coloring problems' and was reviewed in detail [40,41].

The intracluster contacts range from 3.023(1) to 3.196(1) Å for **I** and from 3.020(1) to 3.077(1) Å for **II**. They are intermediate to the corresponding distances in Sr_3Sn_5 (2.99 – 3.15

Å) [18] and Sr_3Tl_5 (3.11 – 3.45 Å, see below). The shortest intracluster contacts are observed between atoms of the pyramidal bases. The basal planes of the pyramidal clusters deviate slightly from planarity with dihedral angles of 8.31° and 8.17° for **I** and **II**, respectively. These values are significantly lower compared to the angles found in Sr_3Tl_5 (13.7°, below) or Sr_3Sn_5 (10.3°). In first coordination the clusters are surrounded by 14 Sr atoms that approximately adopt the shape of a hexacapped quadrangular prism (Figure 3c).

The Sr1 atoms are nine–fold coordinated with contacts to clusters of four different chains (d(Sr1–M) = 3.266(1) – 3.608(1) Å for **I** and 3.264(2) – 3.603(2) Å for **II**). Sr2 is nested in the spaces between the zigzag cluster chains with contacts to 10 M atoms (d(Sr2–M) = 3.418(1) – 3.540(1) Å for **I** and 3.413(1) – 3.538(1) Å for **II**).

3.2 Structure Description for III and IV. Both compounds crystallize in the prominent Pu_3Pd_5 structure type. The projection of the unit cell of Ca_3Tl_5 (Figure 1c), with cluster representation of the thallium substructure, shows that the clusters are aligned in zigzag chains (along c) which are orientated parallel to each other. Crystallographically defined C_{2v} square pyramidal clusters made of Tl1 to Tl3 with intracluster Tl–Tl distances of 3.157(1) – 3.492(2) for **III** and 3.107(2) – 3.447(3) Å for **IV** are recognizable (Figure 2b). Like in **I** and **II** the shortest intracluster bonds are found between the three–bonded atoms of the pyramidal base (3.157(1) Å in **III** and 3.107(2) Å in **IV**). These values are in good agreement with twice the metallic single bond radii for Tl (3.11 Å) [42] and they lie in the range of covalent interactions reported for other thallium clusters with comparable low oxidation numbers [10]. In both cases bonds between the apical Tl1 and the basal Tl atoms are significantly longer with values ranging from 3.246(2) to 3.492(2) Å in **III** and 3.227(3) to 3.447(3) Å in **IV**. The pyramidal base deviates from planarity with dihedral angles of 13.36° and 13.68° for **III** and **IV**, respectively.

In contrast to **I / II** the clusters are interconnected *via* all vertices (Figure 1c, dashed lines) with *exo*–bonds ranging from 3.426(2) to 3.499(2) Å for **III** and from 3.560(4) to 3.681(2) Å for **IV**. Thus, a 3D cluster network is formed and the higher degree of cluster polymerization is evident as the intercluster distances are approximately in the same range as the longer intracluster bonds (d(Tl–Tl)$_{intra}$ = 3.491(2) Å for **III** and 3.447(3) Å for **IV**). However, this is clearer for Ca_3Tl_5 (d(Tl1–Tl2)$_{inter}$ = 3.427(2) Å) as the length differences of the intercluster bonds in **III** and **IV** are mostly dictated by relative cation sizes.

The coordination spheres around the two types of *Ae* atoms are similar to that found in phases **I** and **II**. In both structure types *Ae*1 is surrounded by six {Tl_5} clusters *via* nine *Ae*–Tl contacts, with average bond lengths of d(*Ae*1–Tl) = 3.31 and 3.46 Å for **III** and **IV**,

respectively. *Ae*2 has contacts to Tl atoms of four pyramids *via* ten *Ae*–Tl contacts, with mean *d*(*Ae*2–Tl) = 3.41 and 3.54 Å for **III** and **IV**, respectively.

3.3 Electronic Structures. Interactions in/between the pyramidal anions and to the cationic array may play a crucial role in the electronic properties of both structure types. Therefore, DFT calculations were performed with the LMTO method.

The DOS for $Sr_3Sn_{5-x}Tl_x$ is calculated for $x = 0$ and the lattice parameters of compound **II**. As shown in Figure 4a the visual nature of the DOS is very similar to the one reported for Sr_3Sn_5 (*Cmcm*) [16,17] and it is consistent with the rather similar crystal structure. Whereas the Fermi level (104 VE/cell) cuts finite DOS, the level corresponding to $x = 2$ with 96 VE/cell cuts the DOS at a deep pseudo gap located −0.5 eV below according to a rigid band approximation. At the pseudo gap only few band crossings are visible along the $\Gamma \rightarrow Z$ direction. Considering the anionic network only, the 96 VE correspond to a count of 24 cluster electrons and thus, an isolated *nido*–cluster $\{Sn_3Tl_2\}^{6-}$ (2*n*+4 skeletal electrons). Considering the two external *M*3–*M*3 intercluster bonds the clusters can be described as (2*n*+6) *arachno*–type $\{Sn_3Tl_2\}^{6-}$. In part, such *exo*–bonds would require involvement of lone pairs essentially of Tl–5*s* character, which is unlikely due to the large 6*s*-6*p* separation. And although the crystallographically determined compositions (x = 1.78 (**I**) and 2.16 (**II**)) are close to this ideal scenario, the intercluster separations are quite long (> 3.4 Å) and cannot be regarded as full 2*c*–2*e* bonds – on the other hand two excess electrons preclude the *nido*–case as well. Nevertheless, as visible from the −COHP diagram in Figure 4a, for 96 VE the anionic interactions are closely optimized in **I** and **II**. Further addition of electrons would destabilize bonding within the anionic clusters, but strengthen the cation–anion interactions.

As shown in Figure 4b and 4c Ca_3Tl_5 and Sr_3Tl_5 are much better metallic conductors. Various bands cross the respective Fermi levels and the transport properties are three dimensional. Between these two compounds there are slight differences: The bands in Ca_3Tl_5 have a higher dispersion than in Sr_3Tl_5 which is visible in the energy range from −10 to −4 eV and originates from smaller radius of Ca and thus shorter intercluster (Table 3) distances. At the same time the interactions between the Tl and the *Ae* atoms increase as some of the Ca–Tl distances are now in the region of even the shorter homoatomic intracluster contacts. The Tl–6*s* states are well separated in the section from −4 to −10 eV below E_F and the broad conduction band shows mainly contributions from Tl–6*p* orbitals (5*d* states occur as a narrow band at ~-12 eV i.e. there is few 5*d*–6*s* mixing/bonding) This feature indicates weak *s*/*p* hybridization, Tl–Tl bonding that is established by mainly the 6*p*-orbitals. The Tl–Tl bonds are roughly optimized at E_F and from the −ICOHP values (Table 5) it can be seen that the

short basal Tl2–Tl3 interactions are clearly the strongest. Interestingly, the averaged Tl–Tl bond is optimized for **III**, whereas for **IV** empty bonding levels exist, which can accept further electrons by a denser cluster matrix or the formation of electron richer isotypes. Additionally, considerable contributions from valence *s*, *p*, and *d* orbitals of the *Ae* atoms mix into the Tl–6*p* and –6*s* bands. Their participation in the bonding is evident (also regarding their number in the unit cell, Table 4). Substantially more unfilled *Ae*–Tl bonding states are present above the Fermi level (up to +3 eV). These bonding terms are on average 0.5 – 0.6 eV per bond for the different Ca–Tl and Sr–Tl contacts and approximately of same magnitudes as the intercluster and the longest intracluster bonds > 3.4 Å (Table 4). Similar cation–anion interactions have frequently been found to significantly add to the bonding energies of a structure [43].

3.4 Discussions. The substitution of atoms by atoms from neighboring groups, under retention of the connectivity in the structure, is a powerful method to evaluate the influence of the valence electron concentration on structure formation [12,13,29]. In the Tm_3Ga_5 and Pu_3Pd_5 structure types, polar intermetallic phases exist which closely approach the electron count expected for the anionic subunits when applying the extended *Zintl–Klemm* formalism including also *Wade's* electron counting rules for deltahedral clusters. The compounds of composition $Ae_3Tt_{5-x}Tr_x$ with discrete five–atom anions have 16–x electrons available for skeletal bonding (skeletal electron = *se*). Thus, for x = 0, such as Sr_3Sn_5, and x = 2 *arachno*–(2×5 + 6 *se*) and *nido*–type (2×5 + 4 *se*) clusters, respectively, are expected. These two five–atom cluster types are rather similar. Only a small displacement of two atoms of the basal square of square-pyramidal clusters leads to an *arachno*–cluster which derives by omitting two corners of a *closo*–pentagonal bipyramid. However, including the longer intercluster bonds two additional *se* are available, which occupy antibonding states in Sr_3Sn_5 and lead to a significant distortion in the pyramidal base [18].

For compounds **I** and **II** the *Zintl* concept leads to the assignments: $(Sr^{2+})_3(Sn_{3.22}Tl_{1.78(5)})^{6-}$ and $(Sr^{2+})_3(Sn_{2.86}Tl_{2.14(5)})^{6-}$ with average *vec* of 4.84 and 4.77, respectively. In terms of *Wade's* rules we obtain *se* numbers between 14.22 and 13.86 for discrete units, which are thus of close to *nido*–type clusters (14 se). Considering two *exo*–bonds per cluster, formally a *arachno*–species with 16 se result and the distortions of the square planes is expected such as for the *arachno*-$\{Sn_5\}^{6-}$ (Sr_3Sn_5, above). However, regarding the *vec* values for the Pu_3Pd_5–type phases, which range from 4.2–5.2 (**Table 1**) or 11–16 *se* for discrete cluster units, electronically there seems to be little reason for the reorientation of the cluster chains.

Therefore, it is important to examine also the fully substituted phases **III** and **IV** which adopt the Pu_3Pd_5–type.

The only reported binary trielide intermetallics, which are *isotypic* with **III / IV** are La_3In_5 and β–Y_3In_5 (*vec*/In = 4.8). These structures are described as $\{In_5\}^{9-}$ clusters that can be classified as *nido*–clusters with 14 skeletal electrons. Although they can structurally be regarded as *Zintl* phases, they have been found to be metallic [25]. Considering also participation of the cations in the bonding, the *Zintl–Klemm* formalism for Ca_3Tl_5 (**III**) and Sr_3Tl_5 (**IV**) can only be a crude approximation. Formally, it leads to the description $(Ae^{2+})_3(Tl_5)^{6-}$. Neglecting the intercluster bonds, 11 *se* are available within the Tl clusters. With respect to *Wade's* rules and assuming *nido*– or *arachno*–clusters this would result in deficiencies of three and five electrons, respectively. Again, evaluations of bond lengths suggest that intercluster bonding have to be considered. Six *exo*–bonds per cluster formally leave 15 *se* which means an intermediate value between a *nido*– and an *arachno*–species. However, this rather localized picture is rivaled by the results of LMTO calculations which show strong metallic properties without any noticeable gap and a stabilizing electron sink. The –ICOHP values for intercluster Tl–Tl and *Ae*–Tl bonds show significant interactions between the Tl clusters and also with the surrounding *Ae* atoms. Further, whereas for the 26 VE units $\{Tt_5\}^{6-}$, such as in Sr_3Sn_5, all the intercluster bonds are longer compared to the intracluster contacts, in the present electron poorer 21 VE $\{Tl_5\}^{6-}$ clusters they are more balanced (average values for Sr_3Tl_5 are biased due to the short Tl2–Tl3 bonds). Therefore, electronically the existence of Ca_3Tl_5 and Sr_3Tl_5 (*vec*/Tl = 4.2) indicates a remarkable flexibility of this structure type (with respect to *vec*) and the lack of electrons for the formation of *arachno*–clusters (which is probably higher due to covalent cation-anion interactions) is accommodated by changing overall Tl–Tl bonding distances in and between the pyramidal clusters resulting in cluster polymerization. The electron lack seems to mostly affect the apical Tl1 atoms and leads to two *exo*–bonds at this position (all other Tl atoms in the cluster are 3*b* and only establish one additional *exo*–bond). However, the bonding between the Tl atoms alone seems to be too weak to control the overall stability. Additional *Ae*–Tl bonding interactions, which are of same strength as the Tl–Tl interactions, further add to the stabilization of the structures. A similar situation is present when comparing $BaSn_3$ [12] and $BaTl_3$ [44]. In the first case isolated columns of Sn octahedra are present, in the second the corresponding building blocks are interconnected.

In summary, **I/II** and **III/IV** favor two different structure types, which electronically is inherently connected with the demand and the available number of *exo*–bonds. Furthermore,

different extends of cation–anion interactions in the two A_3B_5 structure types have be considered [45]. Finally, it should be noted that a "slow first–order phase transition" from metastable β–Y_3In_5 (Pu_3Pd_5–type) to low temperature α–Y_3In_5 (Tm_3Ga_5–type) has been reported [25]. In the present case, the phases were annealed at relatively low temperatures (500 °C) and longer annealing at higher temperatures might have a similar impact.

References

[1] W. B. Pearson, *The Crystal Chemistry and Physics of Metals and Alloys*; Wiley–Interscience, New York **1972**.

[2] H. Schäfer, B. Eisenmann, W. Müller, *Angew. Chem.* **1973**, *85*, 742; *Angew. Chem.*, *Int. Ed. Engl.* **1973**, *12*, 694.

[3] R. Nesper, *Prog. Solid State Chem.* **1990**, *20*, 1.

[4] J. D. Corbett, *Chem. Rev.* **1985**, *85*, 383.

[5] T. F. Fässler, S. Hoffmann, *Z. Kristallogr.* **1999**, *214*, 722.

[6] R. Nesper, *Angew. Chem.* **1991**, *103*, 805; *Angew. Chem.*, *Int. Ed. Engl.* **1991**, *30*, 789.

[7] T. F. Fässler, *Chem. Soc. Rev.* **2003**, *32*, 80.

[8] G. A. Papoian, R. Hoffmann, *Angew. Chem.* **2000**, *112*, 2500; *Angew. Chem.*, *Int. Ed.* **2000**, *39*, 2408.

[9] S. M. Kauzlarich, Ed., *Chemistry, Structure and Bonding of Zintl Phases and Ions*, VCH Publishers, New York **1996**.

[10] J. D. Corbett, *Angew. Chem.* **2000**, *112*, 682; *Angew. Chem.*, *Int. Ed.* **2000**, *39*, 670.

[11] T. F. Fässler, *Z. Anorg. Allg. Chem.* **2006**, *632*, 1125.

[12] (a) S. Ponou, N. Müller, T. F. Fässler, U. Häussermann, *Inorg. Chem.* **2005**, *44*, 7423. (b) S. Ponou, T. F. Fässler, L. Kienle, *Angew. Chem.* **2008**, *120*, 4063; *Angew. Chem.*, *Int. Ed* . **2008**, *47*, 3999.

[13] (a) U. Häussermann, S. Amerioun, L. Eriksson, C. S. Lee, G. J. Miller, *J. Am. Chem. Soc.* **2002**, *124*, 4371. (b) B. Li, J. D. Corbett, *Inorg. Chem.* **2006**, *45*, 8958. (c) B. Li, J. D. Corbett, *J. Am. Chem. Soc.* **2005**, *127*, 926.

[14] T. F: Fässler, C. Kronseder, *Angew. Chem.* **1997**, *109*, 2800; *Angew. Chem.*, *Int. Ed. Engl.* **1997**, *36*, 2683.

[15] T. F. Fässler, S. Hoffmann, *Z. Anorg. Allg. Chem.* **2000**, *626*, 106.

[16] S. Hoffmann, T. F. Fässler, *Inorg. Chem.* **2003**, *42*, 8748.

[17] T. F. Fässler, S. Hoffmann, C. Kronseder, *Z. Anorg. Allg. Chem.* **2001**, *620*, 2486.

[18] F. Zürcher, R. Nesper, S. Hoffmann, T. F. Fässler, *Z. Anorg. Allg. Chem.* **2001**, *627*, 2211.

[19] M. T. Klem, J. T. Vaughey, J. G. Harp, J. D. Corbett, *Inorg. Chem.* **2001**, *40*, 7020.

[20] E. Zintl, *Angew. Chem.* **1939**, *52*, 1.

[21] K. Wade, *Adv. Inorg. Chem. Radiochem.* **1976**, *18*, 1.

[22] M. Rhode, M. Wendorff, C. Röhr, *Z. Anorg. Allg. Chem.* **2006**, *632*, 1195.

[23] S. Gupta, A. K. Ganguli, *Inorg. Chem.* **2005**, *44*, 7443.

[24] S. Budnyk, F. Weitzer, C. Kubata, Y. Prots, L. G. Akselrud, W. Schnelle, K. Hiebl, R. Nesper, F. R. Wagner, Y. Grin, *J. Solid State Chem.* **2006**, *179*, 2329.

[25] J. T. Zhao, J. D. Corbett, *Inorg. Chem.* **1995**, *34*, 378.

[26] S. P. Yatsenko, E. I. Hladyshevsky, K. A. Tschuntonow, Y. P. Yarmolyuk, Y. N. Hryn, *J. Less. Common Met.* **1983**, *91*, 21.

[27] D. K. Seo, J. D. Corbett, *J. Am. Chem. Soc.* **2001**, *123*, 4512.

[28] Y. P. Yarmolyuk, Y. N. Grin, E. I. Gladyshevskii, *Sov. Phys. Crystallogr.* **1977**, *22*, 416.

[29] S. Ponou, S.-J. Kim, T. F. Fässler, *Z. Anorg. Allg. Chem.* **2007**, *633*, 1568.

[30] E. Zintl, S. Neumayr, *Z. Elektrochem.* **1933**, *39*, 86.

[31] A. Iandelli, *Z. Anorg. Allg. Chem*. **1964**, *330*, 221.

[32] *Scale3/ABSPACK*, *CrysAlis RED,* Oxford Diffraction Ltd., Version 1.171.32 **2007**.

[33] (a) G. Sheldrick, *SHELXS–97*, Program for the Solution of Crystal Structures, Universität Göttingen **1997**. (b) G. Sheldrick, *SHELXL–97*, Program for the Refinement of Crystal Structures, Universität Göttingen **1997**.

[34] *X–Shape*, Stoe & Cie GmbH: Crystal optimization program for numerical absorption correction, based on the program *HABITUS* by W. Herrendorf and H. Bärnighausen, Karlsruhe **1993**, Gieben **1996**, Darmstadt **1997**.

[35] (a) G. Krier, O. Jepsen, A. Burkhardt, O. K. Andersen, *TB–LMTO–ASA Program*, Vers. 4.7; Max-Planck-Institut für Festkörperforschung: Stuttgart, Germany 1995. (b) O. Jepsen, O. K. Andersen, *Z. Physik B* **1995**, *97*, 35.

[36] (a) W. R. L. Lambrecht, O. K. Andersen, *Phys. Rev. B* **1986**, *34*, 2439.
(b) P. Löwdin, *J. Chem. Phys.* **1951**, *19*, 1396.

[37] P. E. Blöchl, R. Dronskowski, *J. Phys. Chem.* **1993**, *97*, 8617.

[38] W. Harms, F. Burggraf, M. Daub, I. Dürr, C. Röhr, *Z. Anorg. Allg. Chem.* **2008**, *634*, 2255. And references therein.

[39] L. Pauling, *J. Am. Chem. Soc.* **1932**, *54*, 3570.

[40] J. Burdett, N. J. Lawrence, J. J. Turner, *Inorg. Chem.* **1984**, *23*, 2419.

[41] G. J. Miller, *Eur. J. Inorg. Chem.* **1998**, 523.

[42] L. Pauling, *J. Am. Chem. Soc.* **1947**, *69*, 542.

[43] (a) B. Li, A. V. Mudring, J. D. Corbett, *Inorg. Chem*. **2003**, *42*, 6940. (b) B. Li, J. D. Corbett, *Inorg. Chem*. **2005**, *44*, 6515. (c) S. Ponou, T. F. Fässler, G. Tobias, E. Canadell, A. Cho, S. C Sevov, *Chem. Eur. J.* **2004**, *10*, 3615.

[44] D. K. Seo, J. D. Corbett, *J. Am. Chem. Soc.* **2002**, *124*, 415.

[45] From a model calculation of Sr_3Tl_5 using the crystal parameters of **II**, we observed slightly more unfilled Tl–Tl bonding states and lower average –ICOHP values for the different interactions, if compared to Sr_3Tl_5 in the crystallographically refined structure.

[46] G. Cordier, H. Schäfer, M. Stelter, *Z. Anorg. Allg. Chem.* **1986**, *539*, 33.

Table 1 Overview of some $(Ae,RE)_3E_5$ compounds, their structure types, and *vec*/*E* values.

Tm_3Ga_5–type		***Pu_3Pd_5–type***		***Ba_3Al_5–type***		***$Hf_3Ni_2Si_2$–type***	
compound	*vec*/*E*	compound	*vec*/*E*	compound	*vec*/*E*	compound	*vec*/*E*
$Sr_3Sn_{5-x}Tl_x$ (x ~ 2; **I**, **II**)	~4.8	Sr_3Sn_5 [18,19]	5.2	$Ba_3Al_3Ga_2$ [22]	4.2	Sr_3In_5 [26]	4.2
RE_3Ga_5 (Sc, Y, Tb–Tm, Lu) [25]	4.8	Ba_3Sn_5 [18]	5.2			Ca_3Ga_5 [45]	4.2
α–Y_3In_5 [24]	4.8	Ba_3Pb_5 [18,19]	5.2			$Sr_3Al_{2.6}Ga_{2.4}$ [22]	4.2
		$Ba_3Ge_{2.82}Sn_{2.18}$ [18]	5.2			Sr_3In_4Pb [22]	4.4
		Eu_3Ge_5 [24]				$Ca_3Al_{1.8}Ga_{3.2}$ [22]	4.2
		La_3In_5 [19]	4.8			$Sr_3Al_{1.8}In_{3.2}$ [22]	4.2
		β–Y_3In_5 [24]	4.8				
		Ca_3Tl_5 (**III**)	4.2				
		Sr_3Tl_5 (**IV**)	4.2				

Table 2 Crystallographic data for $Sr_3Sn_{3.22}Tl_{1.78(4)}$ (**I**), $Sr_3Sn_{2.84}Tl_{2.16(5)}$ (**II**), Ca_3Tl_5 (**III**), and Sr_3Tl_5 (**IV**).

empirical formula	$Sr_3Sn_{3.22}Tl_{1.78(4)}$ (**I**)	$Sr_3Sn_{2.84}Tl_{2.16(5)}$ (**II**)	Ca_3Tl_5 (**III**)	Sr_3Tl_5 (**IV**)
fw / g·mol^{-1}	1008.39	1040.95	1142.09	1284.71
Space group, *Z*	*Pnma* (No. 62), 4		*Cmcm* (No. 63), 4	
Unit cell parameters / Å	*a* = 13.422(1)	*a* = 13.482(2)	*a* = 10.231(2)	*a* = 10.592(5)
	b = 10.897(1)	*b* = 10.938(2)	*b* = 8.362(2)	*b* = 8.667(5)
	c = 6.897(1)	*c* = 6.850(1)	*c* = 10.623(2)	*c* = 10.973(6)
V / Å^3	1008.7(1)	1010.1(2)	908.8(3)	1007.3(9)
T / K	293(2)			
μ / mm^{-1}	51.75	56.79	89.95	95.34
Θ / °	3.32 – 27.82	3.34 – 27.84	4.88 – 25.34	3.04 – 25.33
Reflections integrated	7427	7341	5428	5892
Independent reflections	1254	1254	438	517
	(R_{int} = 0.061)	(R_{int} = 0.093)	(R_{int} = 0.203)	(R_{int} = 0.104)
Reflections $I > 2\sigma(I)$	1128	997	412	361
	(R_σ = 0.035)	(R_σ = 0.054)	(R_σ = 0.068)	(R_σ = 0.056)
Parameter	48	48	27	27
R_1 / wR_2 [$I > 2\sigma(I)$]	0.032 / 0.058	0.038 / 0.065	0.050 / 0.124	0.037 / 0.117
R_1 / wR_2 (all data)	0.040 / 0.060	0.062 / 0.071	0.053 / 0.126	0.057 / 0.121
lgst. diff. peak/hole / e$^-$·Å^3	+1.55/−1.59	+2.06/−1.66	+3.90/−2.84	+3.25/−2.32
Goodness of Fit	1.200	1.104	1.226	1.136

Table 3 Atomic coordinates and equivalent isotropic displacement parameters for $Sr_3Sn_{3.22}Tl_{1.78(4)}$ (**I**), $Sr_3Sn_{2.84}Tl_{2.16(5)}$ (**II**), Ca_3Tl_5 (**III**), and Sr_3Tl_5 (**IV**).

Atom	*Wyck.*	*Occ.* ≠ 1	*x*	*y*	*z*	U_{eq} / Å^2
			I			
*M*1 = Sn1 / Tl1	4*c*	0.55 / 0.45(1)	0.7639(1)	¾	0.1485(1)	0.020(1)
*M*2 = Sn2 / Tl2	4*c*	0.70 / 0.30(1)	0.7928(1)	¾	0.5964(1)	0.021(1)
*M*3 = Sn3 / Tl3	8*d*	0.60 / 0.40(1)	0.9033(1)	0.5544(1)	0.3621(1)	0.019(1)
*M*4 = Sn4 / Tl4	4*c*	0.78 / 0.22(1)	0.9932(1)	¾	0.1052(1)	0.021(1)
Sr1	4*c*		0.5689(1)	¾	0.8653(2)	0.017(1)
Sr2	8*d*		0.8530(1)	½	0.8711(1)	0.018(1)
			II			
*M*1 = Sn1 / Tl1	4*c*	0.42 / 0.58(1)	0.2352(1)	¾	0.1408(1)	0.024(1)
*M*2 = Sn2 / Tl2	4*c*	0.56 / 0.44(1)	0.2092(1)	¾	0.5985(1)	0.025(1)
*M*3 = Sn3 / Tl3	8*d*	0.55 / 0.45(1)	0.0976(1)	0.5544(1)	0.3620(1)	0.022(1)
*M*4 = Sn4 / Tl4	4*c*	0.76 / 0.24(1)	0.0074(1)	¾	0.1065(2)	0.025(1)
Sr1	4*c*		0.4329(1)	¾	–0.1342(2)	0.019(1)
Sr2	8*d*		0.1465(1)	½	–0.1303(2)	0.021(1)
			III			
Tl1	4*c*		0	0.5222(2)	¾	0.037(1)
Tl2	8*g*		0.2141(1)	0.2355(2)	¾	0.034(1)
Tl3	8*f*		0	0.2037(1)	0.5374(1)	0.033(1)
Ca1	4*c*		0	0.088(1)	¼	0.033(2)
Ca2	8*e*		0.2861(6)	0	½	0.035(1)
			IV			
Tl1	4*c*		½	0.5015(3)	¼	0.026(1)
Tl2	8*g*		0.2949(2)	0.2263(2)	¼	0.023(1)
Tl3	8*f*		½	0.1958(2)	0.4510(1)	0.021(1)
Sr1	4*c*		½	0.1150(6)	¾	0.020(1)
Sr2	8*e*		0.2083(3)	0	½	0.018(1)

Table 4 Selected interatomic distances for $Sr_3Sn_{3.22}Tl_{1.78(4)}$ (**I**), $Sr_3Sn_{2.84}Tl_{2.16(5)}$ (**II**), Ca_3Tl_5 (**III**), and Sr_3Tl_5 (**IV**).

Atom pair		Distance	Atom pair		Distance	Atom pair		Distance	Atom pair		Distance
		I						**II**			
*M*1	*M*4	3.091(1)	Sr1	*M*1	3.266(1)	*M*1	*M*4	3.080(2)	Sr1	*M*1	3.264(2)
	*M*2	3.114(1)		*M*3	3.338(1)×2		*M*2	3.155(1)		*M*3	3.355(1)×2
	*M*3	3.196(1)×2		*M*4	3.400(1)		*M*3	3.212(1)×2		*M*4	3.388(2)
*M*2	*M*3	3.059(1)×2		*M*2	3.532(1)	*M*2	*M*3	3.077(1)×2		*M*2	3.529(2)
	*M*1	3.114(1)		*M*3	3.608(1)×2		*M*1	3.155(1)		*M*3	3.603(2)×2
				*M*2	3.715(1)					*M*2	3.733(1)
				*M*4	3.791(1)					*M*4	3.751(1)
*M*3	*M*4	3.023(1)	Sr2	*M*2	3.418(1)	*M*3	*M*4	3.020(1)	Sr2	*M*4	3.413(1)
	*M*2	3.059(1)		*M*4	3.419(1)		*M*2	3.077(1)		*M*2	3.435(1)
	*M*1	3.196(1)		*M*3	3.491(1)		*M*1	3.212(1)		*M*3	3.492(1)
	*M*3	3.429(1)*		*M*1	3.496(1)		*M*3	3.451(1)*		*M*3	3.497(2)
*M*4	*M*3	3.023(1)×2		*M*3	3.504(1)	*M*4	*M*3	3.020(1)×2		*M*1	3.511(1)
	*M*1	3.091(1)		*M*1	3.540(1)		*M*1	3.080(2)		*M*1	3.537(1)
				*M*3	3.624(1)					*M*3	3.594(1)
				*M*4	3.686(1)					*M*2	3.683(1)
				*M*3	3.691(1)					*M*3	3.697(1)
				*M*2	3.694(1)					*M*4	3.713(1)
		III						**IV**			
Tl1	Tl2	3.247(2)×2	Ca1	Tl3	3.203(3)×2	Tl1	Tl2	3.227(3)×2	Sr1	Tl1	3.324(6)
	Tl2	3.427(2)×2*		Tl1	3.260(9)		Tl3	3.447(3)×2		Tl3	3.355(3)×2
	Tl3	3.491(2)×2		Tl2	3.277(4)×2		Tl2	3.681(2)×2*		Tl2	3.413(3)×2
Tl2	Tl3	3.157(1)×2		Tl3	3.324(7)×2	Tl2	Tl3	3.107(2)×2		Tl3	3.481(5)×2
	Tl1	3.247(2)		Tl2	3.480(7)×2		Tl1	3.227(3)		Tl2	3.670(5)×2
	Tl1	3.427(2)*	Ca2	Tl3	3.329(4)×2		Tl1	3.681(2)*	Sr2	Tl3	3.480(3)×2
Tl3	Tl2	3.157(1)×2		Tl2	3.387(2)×2	Tl3	Tl2	3.107(2)×2		Tl2	3.495(2)×2
	Tl1	3.491(2)		Tl3	3.410(5)×2		Tl1	3.447(3)		Tl1	3.521(3)×2
	Tl3	3.499(2)*		Tl1	3.446(4)×2		Tl3	3.560(4)*		Tl3	3.566(4)×2
				Tl2	3.456(1)×2					Tl2	3.627(2)×2

*) intercluster

Table 5 –ICOHP values for selected interatomic contacts in Ca_3Tl_5 (**III**) and Sr_3Tl_5 (**IV**). Energies are given in eV per bond. *n* denotes the number of interactions per unit cell.

interaction		*d* / Å	–ICOHP (at E_F)	–ICOHP (max.)	*n*
			III		
Tl2	Tl3	3.157(1)	1.08	1.08	8
Tl1	Tl2	3.247(2)	0.71	0.74	4
Tl1	Tl2	3.427(2)*	0.56	0.56	4
Tl1	Tl3	3.491(2)	0.46	0.50	4
Tl3	Tl3	3.499(2)*	0.60	0.61	4
Ca1	Tl	3.203(3) – 3.480(7)	0.58	-	36
Ca2	Tl	3.329(4) – 3.456(1)	0.51	-	80
			IV		
Tl2	Tl3	3.107(2)	1.18	1.21	8
Tl1	Tl2	3.227(3)	0.77	0.84	4
Tl1	Tl3	3.447(3)	0.50	0.55	4
Tl3	Tl3	3.560(4)*	0.52	0.54	4
Tl1	Tl2	3.681(2)*	0.35	0.37	4
Sr1	Tl	3.324(6) – 3.670(5)	0.54	-	36
Sr2	Tl	3.480(3) – 3.627(2)	0.49	-	80

*) intercluster

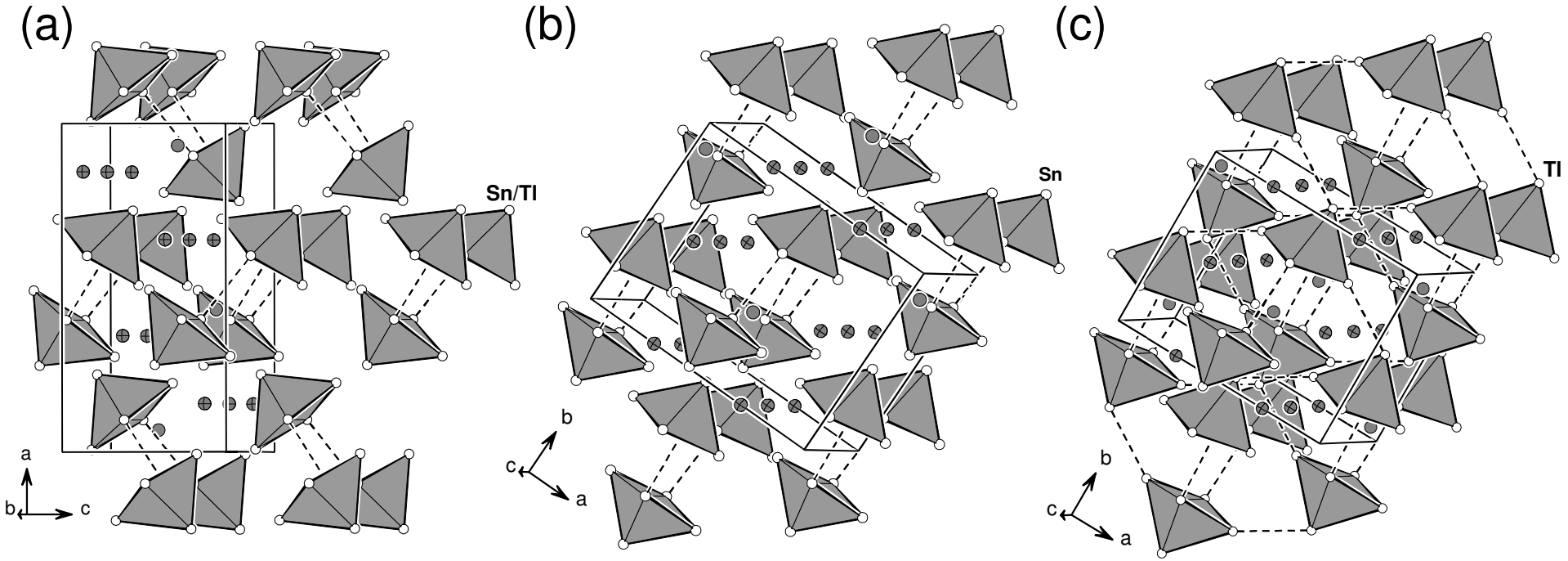

Figure 1. Perspective view of the unit cells of (a) compounds $Sr_3Sn_{3.22}Tl_{1.78}$ (**I**), $Sr_3Sn_{2.84}Tl_{2.16}$ (**II**), (b) Sr_3Sn_5, and (c) compounds Ca_3Tl_5 (**III**), Sr_3Tl_5 (**IV**). In contrast to (b) additional intercluster bonds occur in (c) which are drawn as dashed lines. *Ae* = Sr, Ca are represented as grey (*Ae*2 atoms cross hatched) and Sn, Tl, *M* = Sn/Tl atoms as empty spheres.

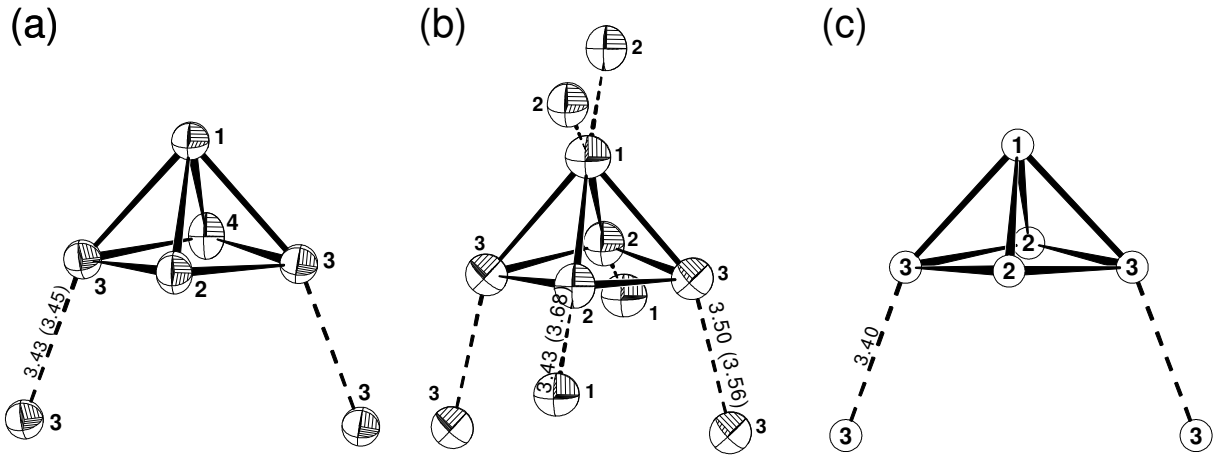

Figure 2. The five–atom cluster and connectivity for (a) $\{M_5\}$ in compound **I**, (b) $\{Tl_5\}$ of compound **III**, (c) and $\{Sn_5\}$ cluster in Sr_3Sn_5. Numbers in parentheses in (a) and (b) denote corresponding intercluster distances [Å] in **II** and **IV**, respectively. Ellipsoids in (a) and (b) are drawn with 90% probability level of the atoms.

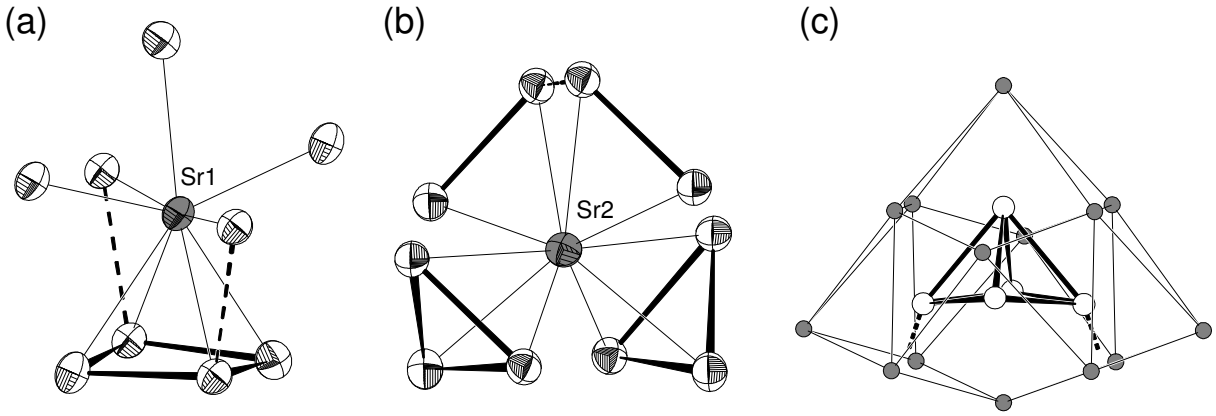

Figure 3. Coordination environments around (a) Sr1 and (b) Sr2. (c) The cation polyhedron around a five–atom cluster. Similar coordination figures are found for all compounds **I** – **IV**. The cutoff value for *Ae–M* and *Ae–Ae* 'bonds' has been set to 4 and 5 Å, respectively. Ellipsoids in (a) and (b) are drawn with 90% probability level of the atoms.

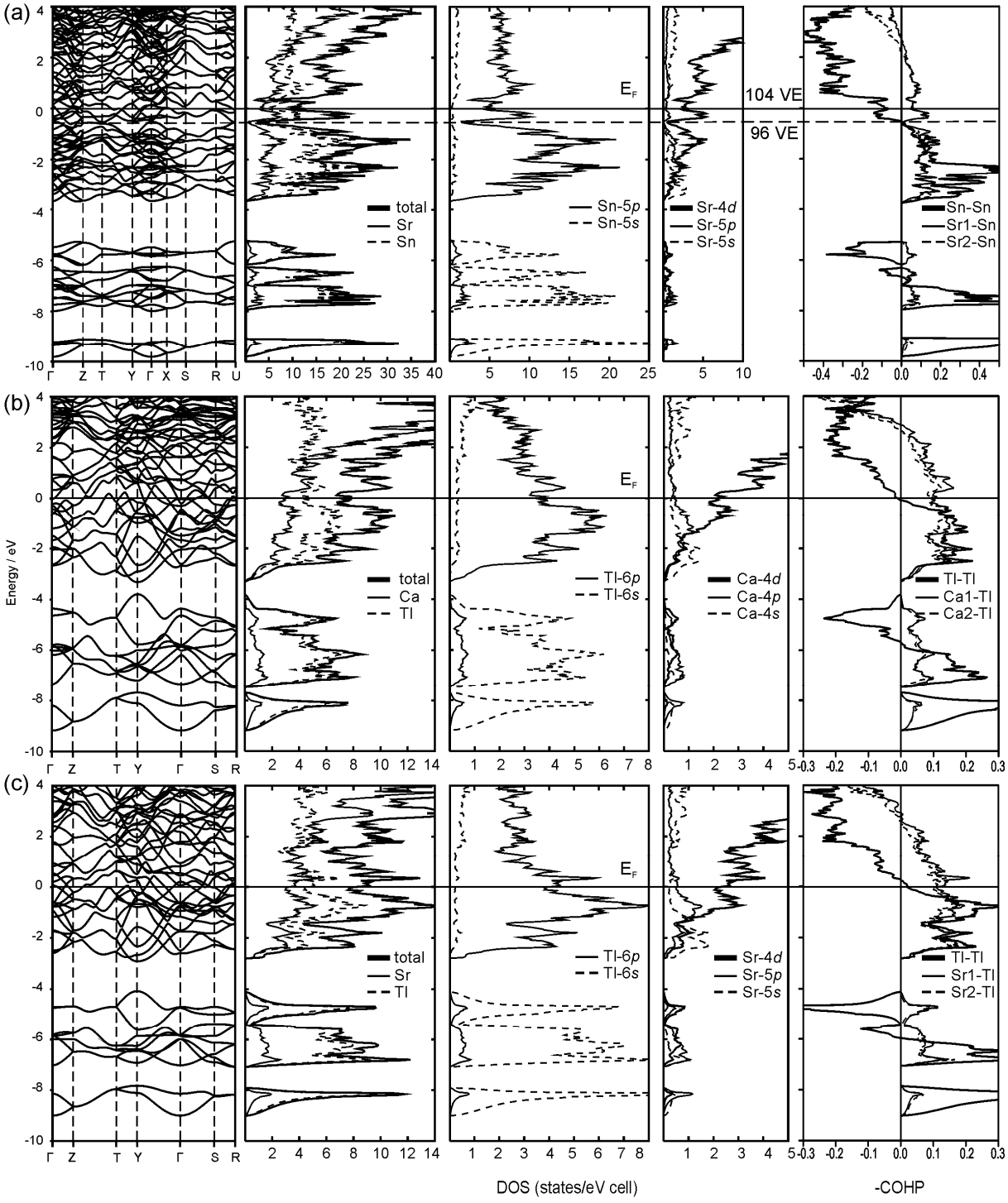

Figure 4. Band structure**,** DOS, and −COHP (averaged) diagrams for (a) $Sr_3Sn_{5-x}Tl_x$ (x = 0 with 104 *VE*/cell) calculated by using the crystal parameters of compound **II**. The *Zintl* limit (x = 2 with 96 *VE*/cell) is indicated. (b) **III**. (c) **IV**. Sn–Sn (Tl–Tl) and *Ae*–Sn (*Ae*–Tl) interactions were considered up to 3.7 and 4 Å, respectively.